

Single-molecule spectroscopy of π -conjugated polymers

Thesis submitted for the degree of
Doctor of Philosophy
by

Oleg Mirzov



**LUND
UNIVERSITY**

Department of Chemical Physics

AKADEMISK AVHANDLING som för avläggande av filosofie doktorsexamen vid naturvetenskapliga fakulteten,
Lunds universitet kommer att försvaras på engelska vid en offentlig disputation på hörsal B, Kemicentrum,
Getingevägen 60, Lund, fredagen den 16 maj 2008 kl 13.15.

Fakultetens opponent är Prof. Lewis Rothberg, Department of Chemistry, University of Rochester, USA

Organization LUND UNIVERSITY Department of Chemical Physics	Document name DOCTORAL DISSERTATION	
	Date of issue April 21 st , 2008	
Author(s) Oleg Mirzov	Sponsoring organization	
Title and subtitle		
Single-molecule spectroscopy of π -conjugated polymers		
Abstract		
<p>When applied to condensed-matter samples of large organic molecules, optical spectroscopy faces the problem of inhomogeneous broadening caused by the diversity of environments and conformations that sample molecules are subjected to. This severely limits the information that can be extracted from optical spectra. Single-molecule spectroscopy offers the most natural way to overcome this problem.</p> <p>π-conjugated polymers are a class of photoluminescent materials whose electronic structure is similar to that of semiconductors, which makes them promising materials for a range of applications. Spectroscopically, they are multichromophoric systems showing individual photophysical properties due to efficient excitation energy transfer to a small number of fluorescent exciton traps. This makes them a natural object to study with single-molecule spectroscopy.</p> <p>This thesis presents a series of results obtained with a range of single-molecule spectroscopy-based techniques on the model conjugated polymer MEH-PPV. Single-chain fluorescence intensity fluctuations (blinking), fluorescence spectral diffusion, fluorescence kinetics and polarization properties have been observed and investigated. Apart from the pristine single-molecule spectroscopy, the range of techniques included: single-molecule imaging (low temporal resolution), time-correlated single photon counting (high temporal resolution) and a novel technique – 2D polarization single-molecule imaging – which is being reported in detail for the first time. Most of the techniques have been combined with temperature-dependent measurements (from 15 K on). Other types of samples (<i>e.g.</i> chain aggregates and submonolayer films) have been studied for comparison, too.</p> <p>In addition, a technique for simulating the photophysical properties of the polymer chains by simple and computationally affordable means is presented.</p>		
Key words Single-molecule spectroscopy, π -conjugated polymers, MEH-PPV, blinking, spectral diffusion, low temperature, fluorescence lifetime, 2D polarization, Monte Carlo, energy transfer.		
Classification system and/or index terms (if any)		
Supplementary bibliographical information	Language: English	
ISSN and key title	ISBN 978-91-7422-193-0	
Recipient's notes	Number of pages 129	Price
Security classification		

Distribution by (name and address): Oleg Mirzov, Dept. of Chemical Physics, Lund University,
P.O.Box 124, 22100 Lund, Sweden

I, the undersigned, being the copyright owner of the abstract of the above-mentioned dissertation, hereby grant to all reference sources permission to publish and disseminate the abstract of the above-mentioned dissertation.

Signature Oleg Mirzov Date April 14th, 2008

Моим близким

Contents

Preface	1
List of Articles	2
1 Introduction	4
1.1 Single-molecule spectroscopy	4
1.2 Π -conjugated polymers	5
1.3 Single-molecule spectroscopy of π -conjugated polymers . .	8
2 Experimental	10
2.1 Sample preparation	10
2.2 Experimental setup	12
3 Data processing	16
3.1 BrightStat	16
3.2 Other software	18
4 Experimental results	21
4.1 From films and solutions to single chains: the difference in spectral properties	21
4.2 Fluorescence spectral diffusion: dispersive interactions in polymer chains	23
4.3 Fluorescence blinking: direct exciton quenching	24
4.4 Time-resolved fluorescence: energy transfer domains . . .	25
4.5 2D polarization single molecule imaging: probing energy transfer	27
5 Modelling and simulations	30
5.1 Monte Carlo simulation of polymer chain conformations . .	30
5.2 Simulations of energy transfer in conjugated polymer chains	31
Bibliography	34
Acknowledgements	36
Articles	39

Preface

This thesis presents the research that the author was involved in together with other members of the single-molecule spectroscopy group of the Department of Chemical Physics during his PhD studies. The thesis is arranged as a collection of articles preceded by an introduction and an overview. Chapter 1 gives a short general introduction into the field of single-molecule spectroscopy of π -conjugated polymers. Chapter 2 presents the experimental techniques. Chapter 3 demonstrates the importance of data processing for the field and gives some examples of home-made software that was produced for that purpose. Chapter 4 contains an overview of the experimental results and main conclusions drawn from them. Every section of Chapter 4 is an introduction to/abstract of an article listed in the end of the thesis. Finally, Chapter 5 summarizes some efforts in simulating polymer chain conformation and photophysical properties numerically.

List of Articles

The articles included in the thesis are listed here, followed by other relevant articles. The choice of articles to be included was determined by intention of making a representation of author's research activity, relevant to the main subject and without duplications. Author's contributions are described with the text in smaller print.

Articles included in the thesis

- I. O. Mirzov, I. G. Scheblykin, "Photoluminescence spectra of a conjugated polymer: from films and solutions to single molecules", *Phys.Chem.Chem.Phys.*, **2006**, 8, 5569 (cover article)
Experimental part, data analysis and most of the manuscript text.
- II. T. Pullerits, O. Mirzov, and I. G. Scheblykin, "Conformational Fluctuations and Large Fluorescence Spectral Diffusion in Conjugated Polymer Single Chains at Low Temperatures", *J.Phys.Chem.B*, **2005**, 109, 19099
Data analysis and a part of the manuscript text. Related to Article VIII (see below).
- III. O. Mirzov, F. Cichos, C. von Borczyskowski, I. G. Scheblykin, "Direct exciton quenching in single molecules of MEH-PPV at 77 K", *Chem.Phys.Lett.*, **2004**, 386, 286
Software development, data analysis and approximately half of the manuscript text.
- IV. O. Mirzov, F. Cichos, C. von Borczyskowski, I. Scheblykin, "Fluorescence blinking in MEH-PPV single molecules at low temperature", *J.Lum.*, **2005**, 112, 353
Data analysis and about half of the writing.
- V. H. Lin, S. R. Tabaei, D. Thomsson, O. Mirzov, P.-O. Larsson, I. G. Scheblykin, "Fluorescence Blinking, Exciton Dynamics and Energy Transfer Domains in Single Conjugated Polymer Chains", **2008**, accepted for publication in *JACS*
Contributed to the development of a physical picture, performed numerical simulations and wrote corresponding parts of the text, developed software for fluorescence decay analysis.

- VI. O. Mirzov, R. Bloem, P. R. Hania, D. Thomsson, H. Lin, and I. G. Scheblykin, “2D polarisation single molecule imaging of multichromophoric systems with energy transfer”, **2008**, Manuscript
Developed most of the key concepts of the new technique, wrote a package of software and the manuscript (except the sample preparation recipe).
- VII. O. Mirzov and I. G. Scheblykin, “Single conjugated polymer chain conformation and excitation energy transfer simulations”, **2008**, Manuscript
Practically all the work, under moderate supervision from I. G. Scheblykin.

Other articles

- VIII. O. Mirzov, T. Pullerits, F. Cichos, C. von Borczyskowski, I. G. Scheblykin, “Large spectral diffusion of conjugated polymer single molecule fluorescence at low temperature”, *Chem. Phys. Lett.*, **2005**, 408, 317
Software development, data analysis and most of the manuscript text. Related to the larger Article II, so Article VIII was not included into the thesis to avoid duplication.
- IX. O. Mirzov, I. G. Scheblykin, “Polydispersity of the photoluminescence quantum yield in single conjugated polymer chains”, *Chem. Phys.*, **2005**, 318, 217
Practically all the work, under supervision from I. G. Scheblykin. The reasoning in the paper was based on a false specification from the polymer manufacturer (polydispersity of 1.06), which compromised the main conclusion, although it may still be true. Nevertheless, the paper was excluded from the thesis.
- X. A. Herland, D. Thomsson, O. Mirzov, I. G. Scheblykin, O. Inganäs, “Decoration of amyloid fibrils with luminescent conjugated polymers”, *J. Mater. Chem.*, **2008**, 1, 126
Largely contributed to the development of a technique and software (Article VI) used in this work. The work lies somewhat outside the main subject, so it was not included into the thesis.
- XI. P. Björk, D. Thomson, O. Mirzov, J. Wigenius, O. Inganäs, I. G. Scheblykin, “Structural studies of a well defined conjugated polyelectrolyte and its interaction with DNA”, **2008**, submitted
Same as in Article X, plus wrote some parts of the manuscript.

Chapter 1

Introduction

1.1 Single-molecule spectroscopy

Conventional optical spectroscopy studies a macroscopic sample with the purpose of obtaining information about sample structure and properties. The sample consists of molecules and, consequently, its spectral properties are determined by the spectral properties of the molecules. The spectral properties of the molecules, in their turn, are defined not only by their structure, but also by the local environment surrounding each of them. Since no macroscopic sample is homogeneous on a microscopic level, this local environment differs from one molecule to the next. Besides, large molecules can have different individual morphology themselves. Therefore, any spectral property of a macroscopic sample, as observed with conventional optical spectroscopy, is a result of some sort of an averaging over the properties of the molecules comprising the sample. This phenomenon is called inhomogeneous broadening. Its main negative effect is the loss of spectral structure and the consequent loss of information about sample properties.

The most natural way to overcome this problem is to study only one molecule as a sample. However, this is an experimental challenge that could not be met until 1989, when the first paper on optical detection of single molecules was published by Moerner and Kador [1]. This work was followed shortly by a contribution from M. Orrit *et. al.* [2] who introduced single-molecule spectroscopy of dye molecules by means of fluorescence excitation in 1990.

One of the most spectacular effects observed with single-molecule spectroscopy is so-called fluorescence intermittency (or blinking effect) [3]. This phenomenon consists in interrupted fluorescence of a single molecule excited with a continuous light source. The reason for fluorescence interruption is a reversible switching of the molecule to a non-luminescent, “dark” state. The nature of the “dark” state depends on the molecule. For example, it can be the first triplet excited state,

which is lower in energy than the first singlet state (Fig. 1.1). Radiative

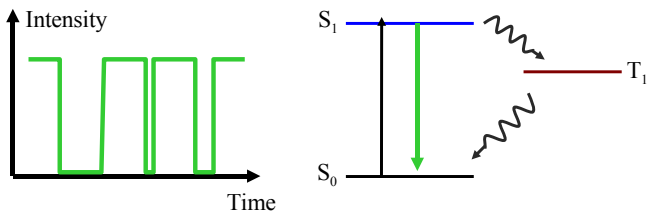


Figure 1.1: Blinking effect in dye molecules.

transition from the triplet state is forbidden, so the molecule can stay in this state for a long time (up to milliseconds or even more depending on the system) without absorption and emission of photons. Then the molecule relaxes back into the ground state non-radiatively and starts fluorescing again.

Another well-known intrinsically single-molecule effect discovered with the new technique was so-called spectral diffusion [4]. This is a phenomenon of absorption frequency change in a single molecule, resulting from a change in its photophysical parameters or a change in local environment. Later it has been shown that fluorescence spectrum of a single dye molecule fluctuates as well [5].

1.2 Π -conjugated polymers

Π -conjugated polymers can be defined as organic polymers with π and π^* molecular orbitals delocalized over the whole polymer chain. In the language of chemical structural formulae, these orbitals are represented as an alternation of single and double carbon bonds along the chain (Fig. 1.2). Another characteristic feature of these formulae is

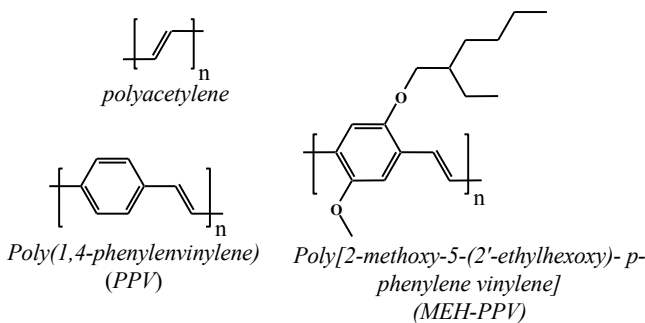


Figure 1.2: Structural formulae of some π -conjugated polymers.

that it is possible to swap the positions of the single and double bonds and end up with a structure that still satisfies the chemical-bonding requirements for carbon.

A lot of research effort has been concentrated on these polymers since the discovery of high conductance in doped polyacetylene [6, 7] by A.J. Heeger, A.G. MacDiarmid, H. Shirakawa, *et. al.* in 1977. In the year 2000 these researchers have been awarded a Nobel Prize in chemistry for this discovery [8]. The reason for such strong interest in π -conjugated polymers is rooted in a unique combination of properties these materials possess.

To get an insight into these properties, it is helpful to consider how π and π^* molecular orbitals are formed from the point of view of the linear combination of atomic orbitals technique (Fig. 1.3c). Two of the

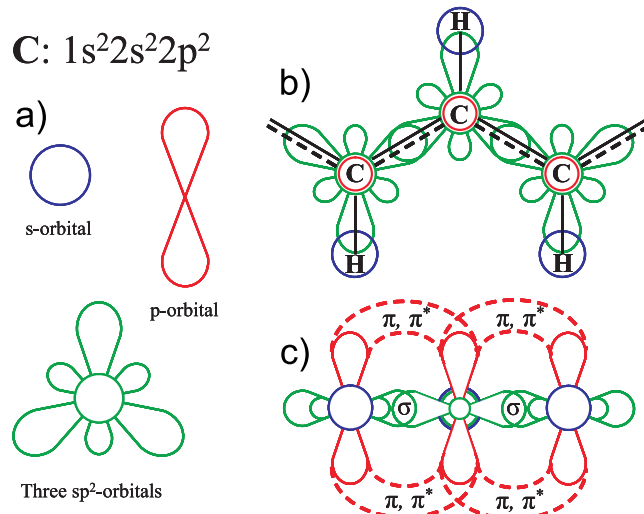


Figure 1.3: A scheme of molecular orbital formation in π -conjugated polymers: a) atomic orbitals of carbon, b) polyacetylene, top view, c) polyacetylene, side view.

three 2p orbitals on each carbon atom combine with the 2s orbital to form three sp^2 hybrid orbitals. These orbitals lie in a plane, are directed at 120° to one another and form three σ molecular orbitals with neighbouring atoms, including one with hydrogen. The third p-orbital on the carbon atom points perpendicular to the sp^2 -orbital plane (Fig. 1.3). It overlaps with the other non-hybrid p-orbitals on neighbouring carbon atoms to form a pair of molecular orbitals: π (bonding) and π^* (anti-bonding). Since electrons can have two different spin states, the lower-energy bonding π -orbital gets occupied, and the higher energy anti-bonding π^* -orbital is left unoccupied. The resulting electronic structure of π -conjugated polymers is similar to that of semiconductors (Fig. 1.4).

Indeed, the highest occupied molecular orbital (HOMO) is analogous

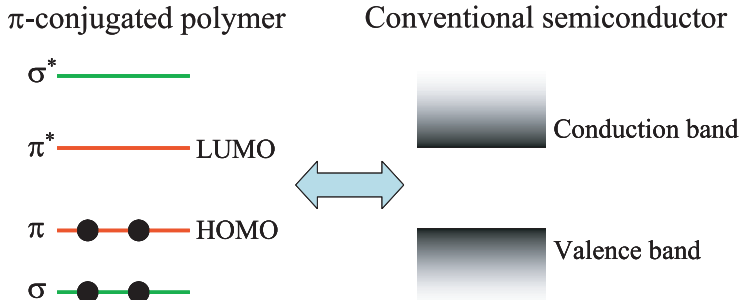


Figure 1.4: The analogy between π -conjugated polymers and semiconductors.

to the valence band edge in semiconductors, the lowest unoccupied molecular orbital (LUMO) — to the conduction band edge, and the gap between them is analogous to the semiconductor band gap. Most conjugated polymers have semiconductor band gaps of 1.5-3 eV, which means that they are suitable for optoelectronic devices that emit visible light. It is the combination of fluorescence and semiconducting properties together with processability of plastics that makes these materials so attractive for applications. In fact, π -conjugated polymers have already found use in organic electronics, photovoltaics and electroluminescent applications as components of organic FETs¹ [9], photovoltaic cells [10] and OLEDs² [11], respectively.

However, the above picture holds only in the ideal case of perfectly straight polymer chains and absence of chemical defects. In reality such imperfections break the conjugation and “chop” the π -orbitals into separate chromophores referred to as spectroscopic units [12] (Fig. 1.5). In the following these two terms will be used synonymously. The typical length of a spectroscopic unit is ~ 5 monomer units

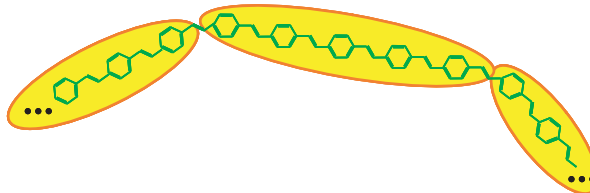


Figure 1.5: Spectroscopic units.

for MEH-PPV [13]. Such a polymer chain is no longer a single semi-

¹FET: field effect transistor.

²OLED: organic light-emitting diode.

conductor “crystal” but a series of chemically bound oligomers with semiconductor-like electronic structure. It was found to be more appropriate to describe electronic excited states in this system in terms of the exciton (correlated electron-hole pair) picture rather than the true band gap (i.e., corresponding to separated, free electron and hole) picture of semiconductors [14, 15].

1.3 Single-molecule spectroscopy of π -conjugated polymers

We have seen that π -conjugated polymers are ensembles of spectroscopic units rather than single light-absorbing chromophores. Therefore, they may seem completely inappropriate objects for studying with single-molecule spectroscopy. Indeed, the ensembles of chromophores they consist of should make them indistinguishable from a bulk material. However, this proved to be wrong with the discovery of fluorescence intensity fluctuations (blinking effect) in single chains of a multichromophoric conjugated polymer [16].

One cannot expect to observe fluorescence blinking from a large ensemble of independent non-interacting chromophores. To explain the blinking effect, it was suggested that there is an efficient dipole-dipole excitation energy transfer (ET) between the spectroscopic units: the excitons in a polymer chain get “funneled” downhill in energy to several (or even only one) spectroscopic units referred to as exciton traps [17]. Every energy funnel can either reversibly switch to a long-lived dark state, or get quenched by an external long-lived quencher [16–18]. The exciton traps have local minima of excited state energy, so the exciton migration is a relaxation process. Hence, the polymer molecule acts as an ensemble of chromophores when absorbing photons, but only a few of the chromophores actually emit light (Fig. 1.6). This fact makes single-molecule spectroscopy a very natural tool to study π -conjugated polymers.

In addition to fluorescence blinking, single π -conjugated polymer molecules were later found to possess very distinct fluorescence spectral properties [19–22] (Article II), exhibit different fluorescence kinetics (Article V) and individual polarization properties (Article VI). This diversity of properties is a further evidence that the chains are different from bulk material and from each other, despite of consisting of a large (~100) number of chromophores. The number of emitting chromophores is much less than the total number, and energy transfer processes are crucial for determining photophysical properties of the polymer chains. Another obvious important factor determining photophysical properties is chain morphology, which in turn depends on polymer synthesis and sample preparation. The above statements can be considered as paradigms of this work and summarized with the di-

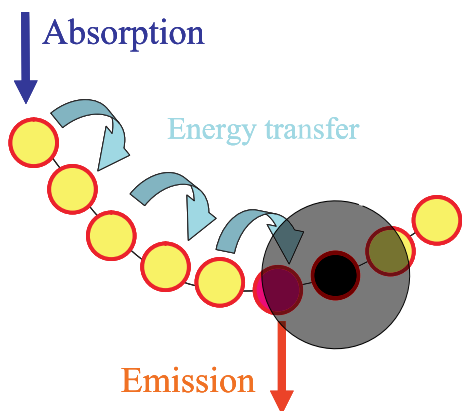


Figure 1.6: Excitation energy transfer to an exciton trap that can get quenched, resulting in fluorescence blinking from the whole chain.

agram shown in (Fig. 1.7):

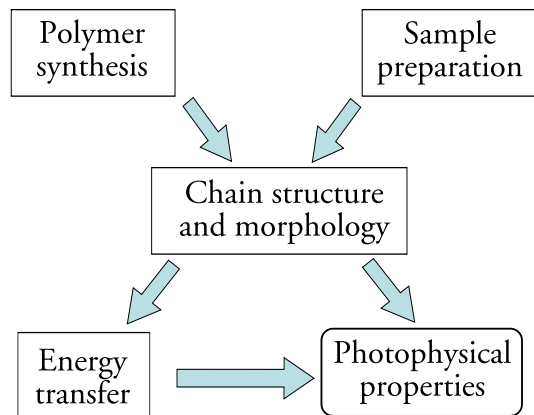


Figure 1.7: Some key paradigms behind this work.

Chapter 2

Experimental

2.1 Sample preparation

Dealing with single molecules suggests that they are present in a very low concentration, and the presence of any fluorescent impurities must naturally be even much lower than that. In practice, it can only be achieved by using highest-purity solvents and taking extreme care of keeping laboratory glassware clean.

Since we are interested in performing optical measurements on single molecules, the molecules should not only be separated from each other so that they do not interact in any way, but also the distance between them should be greater than optical resolution of the experimental setup. In this situation environmental conditions may be somewhat different for different molecules, thereby creating additional inhomogeneous broadening not inherent to the molecules as such. To minimize this effect, one may want to enclose the molecules into a relatively homogeneous chemically inert non-fluorescent polymer host matrix. Alternatively, one can use a cap matrix (Articles II, III, IV) rather than a host matrix, if only protecting the molecules against atmospheric oxygen is important. The typical sample structure is shown in Fig. 2.1.

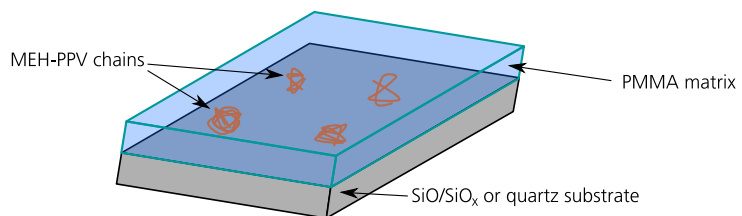


Figure 2.1: The sample structure.

The model π -conjugated polymer MEH-PPV (Fig. 1.2) was chosen as the polymer to be studied. It has the advantage of a simple backbone structure like that of PPV (Fig. 1.2) combined with a good solubility due to the side chains. MEH-PPV was purchased from Sigma-Aldrich and is known to have a number-average molecular weight in the range 150 000–250 000. Host matrices were prepared from poly (methyl methacrylate) (PMMA) and cap matrices — from water-soluble poly (vinyl-alcohol) (PVA). We used oxidized silicon wafers and high-purity quartz plates as substrates.

To prepare the substrates for polymer deposition, a special cleaning routine was applied. First, the wafers were cleaned mechanically with a standard detergent for washing glassware. Then they were rinsed in toluene, dried, and rinsed with deionized water. After that the substrates were kept in a “piranha” mixture (1:2 H₂O₂:H₂SO₄) at \approx 60 °C for \approx 20 minutes to “eat away” any organic impurities. Then the wafers were rinsed with ultra-pure Milli-Q® water very thoroughly. To prevent subsequent precipitation of impurities from the air onto the substrates, they were left to be stored in Milli-Q® water. All the above steps apart from the “piranha” treatment were performed in an ultra-sonic bath. Finally, just before depositing the polymer layers, the substrates were taken out of Milli-Q® water, rinsed once again, dried with a jet of nitrogen and kept under a UV-lamp for half an hour to photobleach the remaining fluorescent impurities.

Polymer solutions for deposition on the substrates were prepared in two steps. First, a matrix solution was prepared (typical concentration was \sim 5 g/L). Then a very dilute (\sim 10⁻⁵ g/L or less) solution of MEH-PPV was prepared by sequential dilution of a stock solution (\sim 1 g/L) and added to the matrix solution (in the case of a host matrix sample) as the final dilution step. Toluene and chloroform were most often used as solvents. To deposit the polymer layers, a standard spin-coating technique was employed. Spin-coating implies either putting a droplet of a solution onto the center of a rotating substrate, or first putting the solution onto the substrate and then spinning it up (Fig. 2.2). In

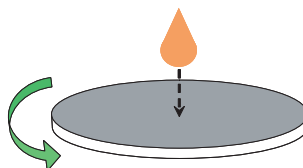


Figure 2.2: An illustration of the spin-coating technique.

this work the latter approach was used. The angular velocity was up to 3000 rpm.

For the case of MEH-PPV chain aggregate samples, a special sample preparation recipe was employed, described in detail in Article VI.

2.2 Experimental setup

One of the possible implementations of single-molecule spectroscopy is called wide-field fluorescence microscopy [23]. The principle of the technique consists in using a fluorescence microscope to study the samples described above. Fluorescence microscope is a microscope used to excite samples with light and to observe the resulting photoluminescence coming from the samples. The advantage of the wide-field approach in comparison with the alternative — confocal microscopy approach [23] — is that no scanning is required, and a large number of molecules can be detected simultaneously. Our setup had three ma-

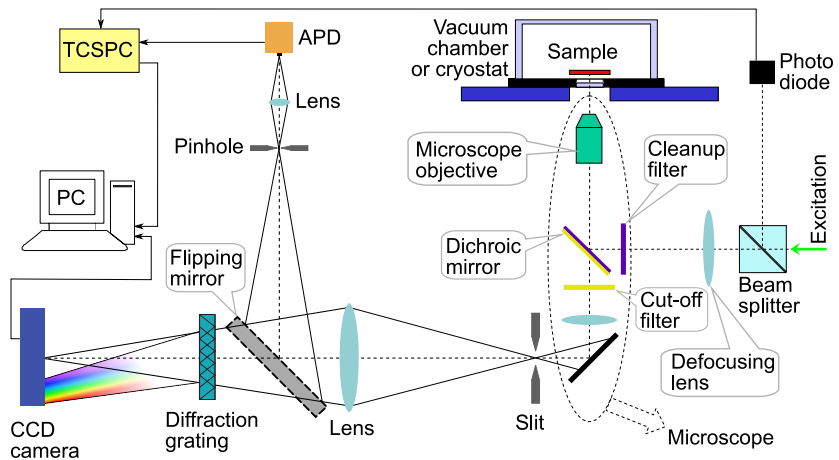


Figure 2.3: A scheme of the experimental setup.

major operating modes: an imaging/spectroscopy mode, a time-resolved mode and a polarization mode. The scheme of the first two is shown in Fig. 2.3. The scheme of the polarization option is shown in Fig. 1 of Article VI, and its photo — in Fig. 2.4 below.

Continuous Ar⁺ laser lines (458, 488 and 514 nm) were used for excitation in the imaging/spectroscopy and polarization modes, whereas for the time-resolved mode frequency-doubled Ti:Saphire laser pulses (≈ 130 fs, 82 MHz) were used. In the latter case, the excitation beam was split in two with a beamsplitter and the reflected component was directed to a photodiode for producing sync pulses (for the imaging/spectroscopy mode, the beamsplitter was not used). Then the beam was steered into the microscope through a defocusing lens and run through the microscope objective (Olympus, LUCPlanFI, 40 \times , N.A. 0.6). The objective had a long working distance (up to 2.3 mm) which gave a possibility of introducing a flat window before the sample (abberation correction). This allowed putting a sample into a cryostat or a vacuum chamber. Vacuum was needed to hinder photooxidation of the sam-

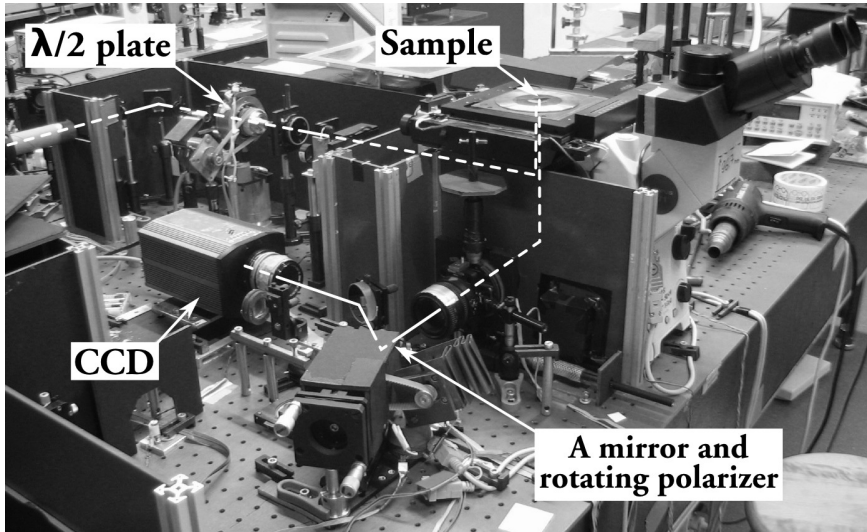


Figure 2.4: A photo of the experimental setup (polarization option).

ple. Due to the defocusing lens, focusing of the excitation beam on the sample was not complete, and the excitation intensity profile in the sample plane had a shape similar to Gaussian, perturbed with diffraction patterns. The typical excitation power density in the maximum of the profile was $\sim 100 \text{ W/cm}^2$.

Fluorescence light was collected with the same objective. A crucial part of the setup is the system of dielectric filters and a dichroic mirror (Fig. 2.3) whose purpose was to separate excitation and fluorescence light. The cleanup filter ensured that only a predetermined excitation wavelength (or a band) would pass through. The dichroic mirror reflected the excitation light but allowed the longer-wavelength fluorescence to pass through towards a detector. The long-pass cut-off filter suppressed the remaining excitation light completely. Fluorescence light was projected through the filters onto a slit to produce an intermediate sample image. The slit served as a spectrometer slit in the case of the spectroscopic setup option.

After the slit, the image was projected with a motorized lens onto a detector: the MPD PDM series single photon avalanche photodiode (APD) in the time-resolved mode or the Photometrics Cascade 512B CCD camera chip in the imaging/spectroscopy mode. The choice between the modes was made with an electrically controlled flipping mirror. If the mirror was up, the sample image was reprojected from the slit plane onto a pinhole whose purpose was to select one molecule to be probed by the APD. The signals from the APD and from the sync photodiode were fed into a PicoQuant time-correlated single photon

counting (TCSPC) module PicoHarp 300. The TCSPC module built histograms of time delays between the sync pulses and the arrivals of photons to the APD. These histograms are essentially fluorescence kinetics curves. They were analyzed to extract the information on the characteristic times of fluorescence and quenching in MEH-PPV single chains (Article V). The instrument response function (IRF) of the whole TCSPC system had a FWHM of 32 ps (inset in Fig. 1 of Article V). Thus, the time-resolved mode allowed studying single-molecule fluorescence with high temporal resolution at the expense of being able to probe only one molecule at a time.

If the flipping mirror was down, the imaging/spectroscopy mode was enacted, and the sample image was projected onto the CCD camera chip. For pure imaging, the projection was direct, and for spectroscopy a holographic diffraction grating was placed between the lens and the CCD, serving as a dispersing element. Such scheme allowed observing a sample image (as the zero order of diffraction) and spectra of the molecules (as the first order of diffraction) simultaneously (see Fig. 2.5). Note that in the case of a single-molecule sample the size of molecule's

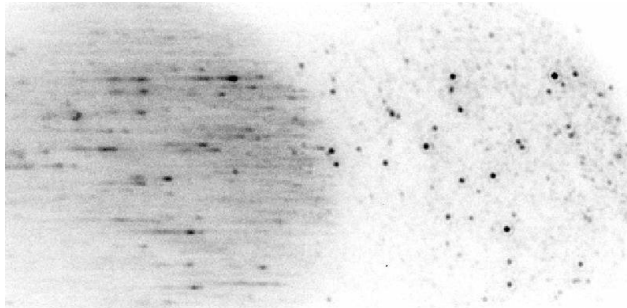


Figure 2.5: Experimental image containing both zero and first orders of diffraction (i.e. the image and spectra) of a single-molecule sample. The slit is opened completely in this case.

image serves as a spectrometer slit by itself (as in Fig. 2.5), whereas in the case of a bulk sample (*e.g.* an MEH-PPV film, see Article I) the slit *must* be used (see Fig. 2.6). The width of the slit determines the spectral resolution in this case¹.

The experimental setup has a limited fluorescence spectral range where it is operational. Besides, even within this range it is not equally sensitive at all the wavelengths. To take this into account, the setup was calibrated using a light source with a known spectrum (a calibration tungsten incandescent lamp). The resulting spectral sensitivity of the setup is shown in Fig. 2.6, top part. All the spectra presented

¹Only up to the highest possible value of ≈ 6 nm which is limited by the size of a CCD pixel.

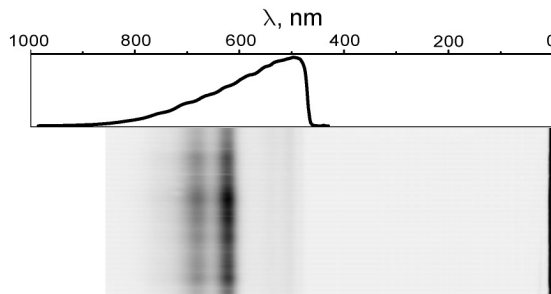


Figure 2.6: Upper part: the spectral sensitivity curve of the experimental setup. Lower part: experimental image containing both zero and first orders of diffraction (i.e. the sample image and spectra) of an MEH-PPV film at 77 K. The slit limits the spectral resolution in this case. The wavelength scale is matched for both parts of the image.

in this work have been corrected with this curve to allow for the non-constant spectral sensitivity.

The camera has a high detection quantum yield, Peltier chip cooling, and a multiplication gain feature for readout noise suppression. These properties allowed achieving high signal-to-noise ratios while taking “movies” with relatively short (fractions of a second) frame acquisition times. Nevertheless, the CCD acquisition times are still very long in comparison with the temporal resolution of the TCSPC option, and only very slow kinetics could be recorded in the “movies”. However, the advantage of using a CCD is the ability to measure spectra and to probe a large (up to a few hundred in the pure imaging mode) number of single molecules at the same time.

Chapter 3

Data processing

The field of single-molecule spectroscopy requires extensive data processing due to dealing with low signal-to-noise ratios and because the raw experimental data do not allow direct interpretation and presentation and need to be analyzed to extract more meaningful information. Many home made data analysis programs have been written during this work, but most of them are beyond the scope of this introduction (and the field, too), so we shall consider only the working principles of one of them — the molecule image detection and intensity tracing program with internal name BrightStat, and briefly describe some others.

3.1 BrightStat

The purpose of BrightStat program (Fig. 3.1) is to analyze the “movies” obtained as the results of imaging with CCD. The acquisition was operated with program WinSpec from the CCD manufacturer Roper Scientific and stored in a format SPE with open specification. BrightStat program was designed to open SPE “movies”, detect the images of molecules, calculate their intensities as integral signals and trace the intensities through the “movies”. The program allows taking non-constant excitation profile into account by loading it from a separately measured profile image, so that every molecule can have an excitation power density value associated with it. Operational region of interest (ROI) of the image can be chosen either as an area where excitation intensity is above some threshold or, in the case when excitation profile is not used, as a user-selected elliptic area.

Detection of molecule images is performed by applying several sequential criteria as follows.

1. All the pixels with local signal maxima are identified within a ROI.
2. A mean μ and a standard deviation σ of pixel signals are calculated, and only those of the local maxima are selected that

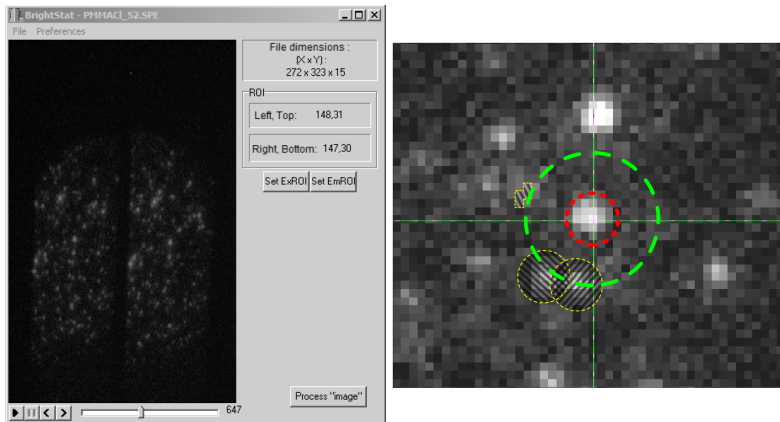


Figure 3.1: Home made image processing software BrightStat: a screen shot (left) and an illustration of some working principles (right).

are higher than $\mu + n_\sigma\sigma$, where n_σ is a user-selected parameter, typically ~ 3 . However, this approach can only narrow down the search for molecules, so after that another criterion is applied to every remaining local maxima as follows.

3. A brightest pixel adjacent to the local maximum is identified. Then another brightest pixel adjacent to the two is found. Then the brightest neighbour of the tree pixels is located, and so on up to a certain user-defined number of pixels (e.g. 8). Then the distance between two most separated pixels of the group is calculated and compared with a user-defined threshold value (e.g. 2.24). If the distance is below the threshold, it means that all the bright pixels are clustered together, so this group is likely to represent a molecule. If the procedure results in “wandering away” from the maximum, it may mean that either this maximum was just a random fluctuation, or that in this spot two molecules happen to have their images “fused together”, which means that this bright area must be disregarded.
4. A Pearson’s r correlation is calculated between the intensity of the pixels around the maximum and their distance from the maximum. For a true image of a molecule, the correlation should be negative, with absolute value above some user-defined threshold (e.g. 0.6).

Taken together, the above criteria compose a quite robust way of detecting the molecules. By adjusting the user-definable parameters, the program can be applied to samples with a wide range of intensities and densities, observed with different optical system magnifications (which results in different single-molecule image sizes).

After the molecules are detected, all the bright areas (satisfying the criterion 2 above) that were not classified as molecules are marked. Then the intensity of every detected molecule is calculated as a sum of the pixel signals within some (again, user-definable) distance from molecule's image maximum. However, we must also subtract a background from this sum, and the background is uniform neither globally (across the image) nor even locally (in the neighbourhood of the molecule of interest). To allow for that, the background was calculated by averaging pixel signals in a ring around the molecule, right), but the other molecules and bright areas were excluded from these statistics (Fig. 3.1).

Extension of the above procedure from a single frame to the whole "movie" is straightforward. Initially, the first frame (or several first frames) are used to identify all the molecules present in the "movie", and then they are traced through. A thorough analysis of every image in the movie with the criteria above (except of the first one) still has to be performed to account for possible appearance of undetected (due to blinking) molecules, to be able to take them into account when calculating background. BrightStat also has an ability to trace moving molecules in fluctuating images, which was very useful for analyzing samples subjected to thermal drifts in a cryostat (Articles III, IV, VI) or images reflected from a rotating polarizer (Article VI).

3.2 Other software

To give a further demonstration of the need for advanced data processing in the field of single-molecule spectroscopy, some other software is briefly described below.

Extracting spectra

In addition to BrightStat which can be used for pure imaging and polarization modes, another program was written for analogous purposes in the spectroscopy mode. The program allows a user to select a molecule's image and corresponding spectrum on one frame and get a series of spectra out, calibrated by wavelength and sensitivity. Operation in bulk mode is also supported for continuous samples (*e.g.* films), when the slit (Fig. 2.3 and 2.6) is used to limit the width of spectral IRF. In addition, spectra fitting feature was also included (Section 4.2 and Article II). This program, as well as BrightStat, was produced with Borland C++ Builder.

Deconvolution problem

Due to a limited temporal resolution of the time resolved option of our setup (Section 2.2) the results of the TCSPC measurements are not the

true kinetic curves of our molecules but convolutions of the true curves with the temporal IRF $A(t)$ (Fig. 1 of Article V, inset):

$$I_{\text{exp}}(t) = \int_{-\infty}^{\infty} I_{\text{true}}(\tau)A(t - \tau)d\tau. \quad (3.1)$$

Deconvolution is a well-known problem with no unique solution. The standard approach to solve it is not to try to extract $I_{\text{true}}(t)$ directly, but to find some model function for $I_{\text{true}}(t)$ that would fit to the experimental $I_{\text{exp}}(t)$ after reconvolution with experimentally measured $A(t)$. There was no ready software available that would allow to use an arbitrary model for fitting, so a new program had to be developed. As a criterion for fitting procedure, maximum likelihood estimation [24] was used. The count values in the bins of a histogram obtained with TCSPC are discrete and Poisson-distributed:

$$w_{\lambda}(k) = \frac{\lambda^k e^{-\lambda}}{k!}, \quad (3.2)$$

where λ is the mean of the distribution. So, maximizing likelihood or, which is the same, maximizing its logarithm, is equivalent to maximizing

$$\ln P = \ln \prod_i p_i = \ln \prod_i \frac{\lambda_i^{k_i} e^{-\lambda_i}}{k_i!} = \sum_i (k_i \ln \lambda_i - \lambda_i - \ln k_i!), \quad (3.3)$$

where k_i are the experimental counts and λ_i come from the model being fitted. The last term in the parentheses in Eq. 3.3 is constant, so fitting criterion is equivalent to minimization of

$$\sum_i (\lambda_i - k_i \ln \lambda_i). \quad (3.4)$$

The expression in Eq. 3.4 was minimized by the fitting procedure, but to estimate the goodness of fit in more practical terms, χ^2 [24] per histogram channel was used. This program has been developed with Matlab technical computing language.

Polarization data

The biggest data processing project within this work was related to polarization measurements (Article VI). A whole toolchain has been developed that takes SPE-“movies” as input and delivers model fit results for polarization 2D plots of series of single molecules. It is done in the following series of steps (see Article VI for more explanations):

1. BrightStat is applied to extract fluorescence intensity transients (for both images: \parallel -polarized and \perp -polarized) and sync signals from experimental “movies”.

2. A Matlab script is used to identify molecule image couples from \parallel -polarized and \perp -polarized subimages.
3. Polarization 2D plots are built from the transients of the couples and the sync pulses.
4. A two-step, 2+8 parameter fitting procedure is applied to fit a model to the 2D plots.
5. The fitting results are further analyzed to extract more physical characteristics of single-molecule polarization properties.

Apart from the first step, all the toolchain has been developed with Matlab.

Chapter 4

Experimental results

4.1 From films and solutions to single chains: the difference in spectral properties

Studying π -conjugated polymers with single-molecule spectroscopy has at least two purposes: purely scientific interest (“what happens if we take single chains and shine some light on them?”) and practical applications (“what is going on in these polymers and how can it be controlled and used?”). For the latter purpose, it is important to know how much the results obtained with single-molecule spectroscopy are relevant to films, because it is in the form of films that conjugated polymers are used in practical applications, such as OLEDs and FETs. However, it is also interesting for the fundamental science to know whether there is a difference between photophysical properties of single chains and films, and if there is some, then where does the crossover occur?

To learn about that, we have investigated a series of samples prepared from solutions of different concentrations (and ranging from single-molecule samples to bulk films) at low temperature (Article I). The key result is schematically presented in Fig. 4.1: as the solution concentration went down (and so did the thickness, naturally), fluorescence spectra shifted to the blue and their band structure became more and more blurred. In order to characterize the observed spectral changes quantitatively, sums of three Gaussian peaks were fitted to the graphs. The peaks represented the vibronic progression (0–0, 0–1 and 0–2 transitions). To characterize the effect of film thickness variation, it is convenient to introduce average intermolecular distance (see Article I for details). After doing so, the average intermolecular distance can be correlated to *e.g.* the position of the 0–0 peak, as it is shown in Fig. 4.2. As one can see, there is a very substantial (≈ 2000 cm^{-1}) spectral shift between the spectra of a thin film and an ensemble of single chains. At high and low intermolecular distances the spectral positions saturate, and the transition from one level to the other

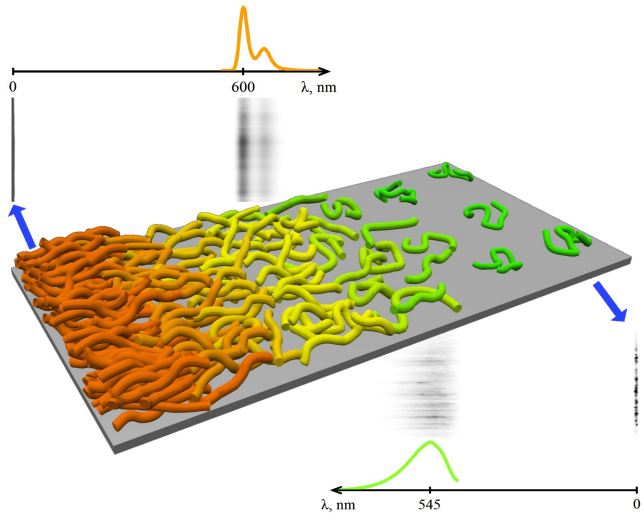


Figure 4.1: A schematic illustration showing the key experimental observation of Article I: MEH-PPV films and ensembles of single chains exhibit different fluorescent spectra.

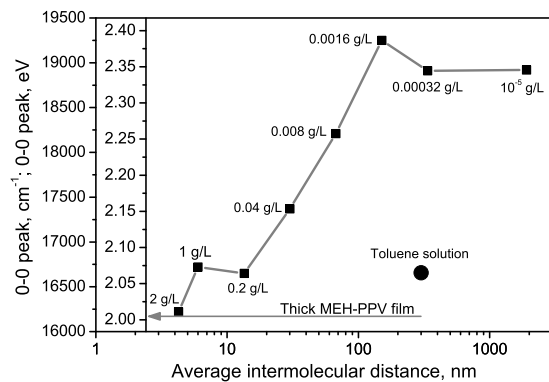


Figure 4.2: Fluorescence spectrum 0–0 peak position of MEH-PPV films (■) and dilute solution (●) as a function of the calculated average intermolecular distance.

occurs most rapidly at around 40 nm. This result clearly shows that photophysical properties of single-chain and bulk samples are quite different, and that care must be taken when generalizing any single-chain results to a polymer as such. In Article I we consider the above key experimental observation in the light of comparison with various literature data and a set of spectroscopic measurements on bulk samples (films and solutions) at room and low temperatures. The main

conclusion is that the reason for the observed effect (Fig. 4.2) is higher conformational disorder in single chains in comparison with that in films and solutions.

4.2 Fluorescence spectral diffusion: dispersive interactions in polymer chains

Now, after some distinctions of isolated molecules from “bulk” samples have been considered (Section 4.1), we can turn to purely single-molecule effects. It turned out that apart from fluorescence blinking (Sections 1.3, 4.3), MEH-PPV exhibited fluorescence spectral diffusion, too [21, 22]. An example of an experimentally observed time-dependence of fluorescence spectrum is shown in Fig. 4.3 (temporal resolution is 0.3 s). As one can see, both 0–0 and 0–1 vibronic peak

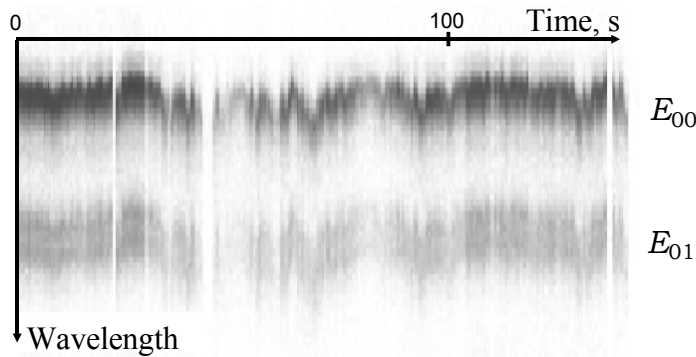


Figure 4.3: Fluorescence spectrum fluctuations in a single MEH-PPV molecule.

shift their positions synchronously, so that the overall spectral shape is preserved. To characterize the observed spectral diffusion quantitatively, 0–0 and 0–1 vibronic peaks of the spectra were approximated with two Lorentzian (Fig. 4.4). This allowed observing spectral position as a function of time. The diffusion range (defined as a difference between the lowest and the highest observed spectral positions) reached as much as 1000 cm^{-1} in cap-matrix samples (Article II). After considering various possible mechanisms of this phenomenon and performing estimating quantum chemical calculations, we arrived at a conclusion that the most likely candidate mechanism is thermal fluctuations of the environment (cap matrix) causing changes in dispersive interactions [25] within polymer chains. The dispersive interactions shift vibronic transition energies. Consequently, their fluctuations can cause the observed fluorescence spectral diffusion.

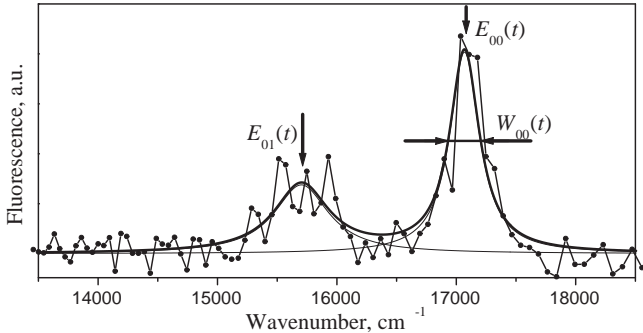


Figure 4.4: The fitting procedure and resulting parameters.

4.3 Fluorescence blinking: direct exciton quenching

Apart from spectroscopy, pure imaging or single polymer chain fluorescence has also proved to be an informative technique. The key background experimental evidence in single-molecule spectroscopy of π -conjugated polymers that we have started our work on Articles III and IV from has been shortly summarized in the introductory chapter (Section 1.3). That evidence is a presence of fluorescence intermittency (or blinking) in single chains of conjugated polymers, despite the fact that they consist of many chromophores. The explanation to that was an assumption of efficient downhill energy transfer to a few fluorescent exciton traps that could be efficiently quenched (Fig. 1.6). However, energy transfer in disordered systems is known to be a temperature-activated process [26]. Therefore, it can be an interesting check to try to observe blinking at low temperature, when energy transfer should be suppressed. In this case, the chains should become more “multichromophore-like”, and blinking should become less pronounced, if not disappear altogether. To evaluate the temperature effect quantitatively, we have introduced the relative fluorescence intensity fluctuation amplitude $\delta F = \Delta F/B$ (Fig. 4.5b, see Article III for more details). For a full on/off fluorescence blinking $\delta F = 1$, and for a constant or monotonously decreasing fluorescence $\delta F = 0$. We have measured fluorescence intensity transients for series of single MEH-PPV chains at room temperature, 77 K (Article III) and 15 K (Article IV), and characterized every transient by its δF and highest intensity value B . The resulting scatter-graphs are shown in Fig. 4.6 for comparison.

As one can see from the graphs, some temperature effect is present (at room temperature, the points tend to concentrate at higher values of δF more than at low temperatures), but it is very limited. It means that the role of energy transfer for blinking effect is small (at least, for

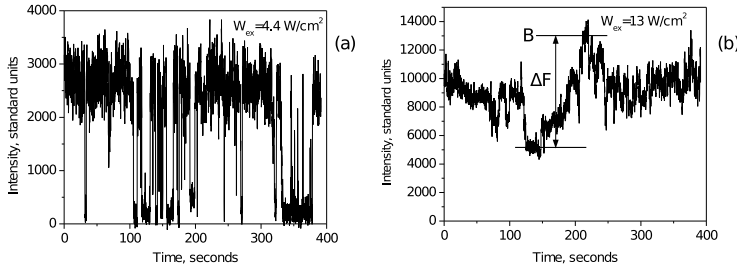


Figure 4.5: Single-molecule fluorescence intensity transients of MEH-PPV: (a) on-off behaviour, (b) irregular amplitude fluctuations. The temporal resolution is 100 ms.

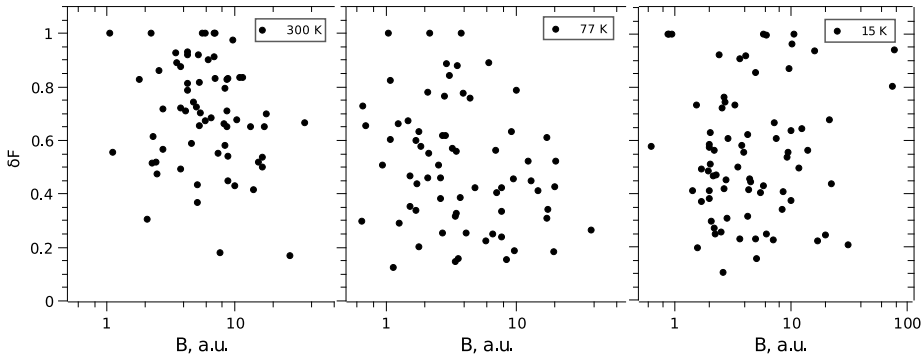


Figure 4.6: Fluorescence intensity fluctuation amplitude δF plotted against brightness B for three different temperatures.

samples prepared as described in Articles III and IV). In that case, how can blinking still be present? One possible answer is illustrated in Fig. 4.7. A quencher may have a very limited quenching radius and energy transfer may be limited to a short range, but in the case if molecule has a collapsed conformation (which is likely to be the case for single MEH-PPV molecules spin-cast from toluene [18,27]), a substantial part of chromophores may be in range, resulting in a noticeable (and possibly even 100%) blinking.

4.4 Time-resolved fluorescence: energy transfer domains

Previously, we have investigated the phenomenon of single-molecule fluorescence blinking in MEH-PPV by studying temperature dependence of fluorescence transients with low (100 ms) temporal resolution

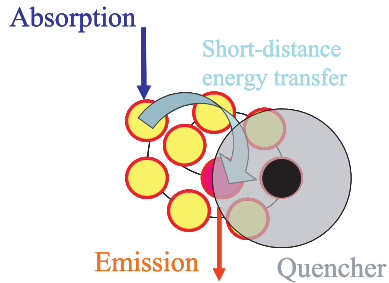


Figure 4.7: In the case of collapsed conformation fluorescence blinking may be observed irregardless of the presence of energy transfer.

(Section 4.3, Articles III and IV). Another aspect to look at might be fluorescence kinetics with picosecond resolution. Fluorescence kinetics reflect processes such as excitation energy transfer (ET) and quenching, so it is of particular interest to see if there is any difference between single-chain fluorescence kinetics in quenched and unquenched states (Fig. 4.8). The time-resolved option of our setup (Fig. 2.3) al-

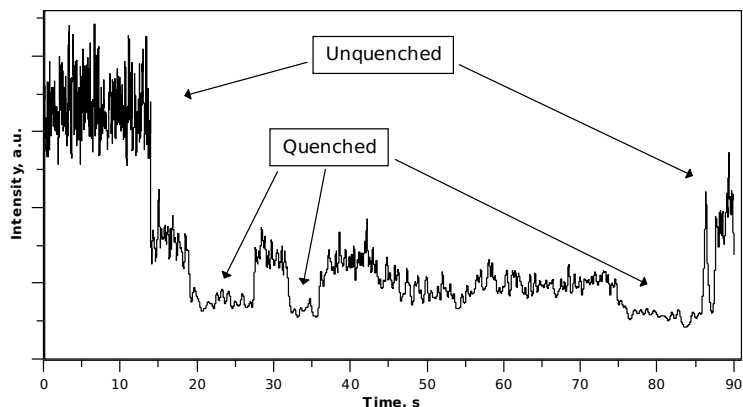


Figure 4.8: Fluorescence intensity transient of a molecule going reversibly to a partially quenched state.

lows measuring fluorescent intensity transients (*e.g.* Fig. 4.8) and kinetics (Fig. 4.9) simultaneously. There is a drastic difference between the unquenched and quenched kinetics: while the former are single-exponential with ~ 600 ps lifetime, the latter kinetics were found to be two-exponential, with slower components of a similar lifetime and much faster ones, ~ 50 ps. As it is discussed in detail in Article V, the conclusion following this observation is that polymer chains are partitioned into zones, or domains, that can be either (almost) unaffected

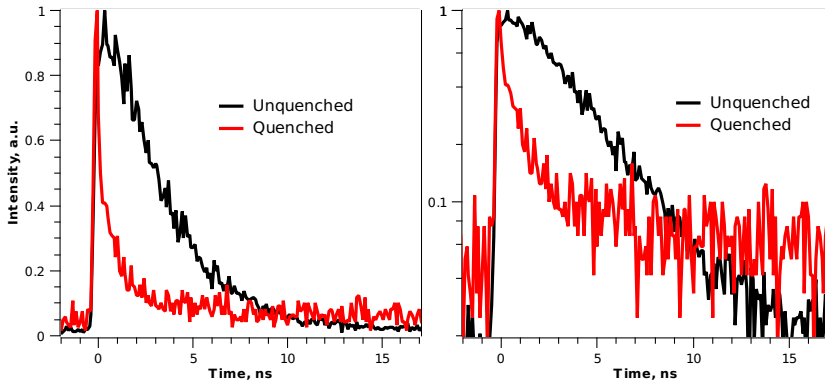


Figure 4.9: Fluorescence decay kinetics in the quenched and unquenched states: linear scale (left) and logarithmic scale (right).

by quencher, or quenched by almost 100%, giving rise to the slow and fast components, respectively (Article V, Fig. 6). This is possible if the following two additional assumptions are correct. Firstly, ET is efficient within the domains but inefficient across them. Secondly, not only downhill ET is present in the polymer chains, but uphill ET as well, though it is less likely. As a result, downhill ET to lowest exciton energy levels is not irreversible: although exciton spends most of its lifetime on the traps, it still visits higher-energy chromophores of the domain, too. Thus, exciton is “delocalized” over the domain and can get quenched efficiently even if only a part of the domain is within a quenching radius of a quencher.

4.5 2D polarization single molecule imaging: probing energy transfer

As it was formulated in (Section 1.3), chain conformation and excitation energy transfer are two key factors determining photophysical properties of π -conjugated polymers. It is not possible to probe polymer chain conformation directly. One possibility of probing it indirectly would be to use the fact that the spectroscopic units that polymer chains consist of (Fig. 1.5) are chromophores with transition dipoles oriented along the polymer backbone. It means that emission from every spectroscopic unit is completely polarized (Fig. 4.10, top). Emission from a system of spectroscopic units can be

- either completely polarized in the case if they are perfectly aligned
- or completely depolarized if they are randomly oriented, covering all the possible orientation directions uniformly,

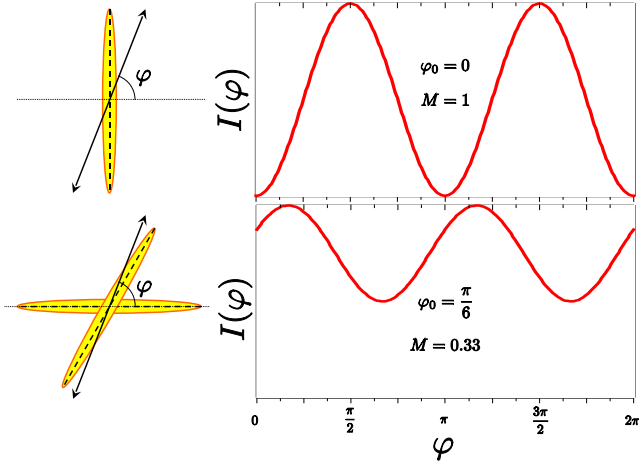


Figure 4.10: Polarization angle dependence of fluorescence intensity from one and two dipoles. In a general case, it has the form $I(\varphi) \sim 1 + M \cos[2(\varphi - \varphi_0)]$.

- or exhibit some intermediate polarization degree (Fig. 4.10, bottom).

An interesting property of polarization dependence of fluorescence intensity is that it always has the functional form

$$I(\varphi) \sim 1 + M \cos[2(\varphi - \varphi_0)], \quad (4.1)$$

where $0 \leq M \leq 1$, $0 \leq \varphi \leq \pi$, $0 \leq \varphi_0 \leq \pi$. Here φ is the polarization plane angle of analyzing polarizer, M — polarization modulation depth and φ_0 — polarization modulation phase.

An important fact is that all the above is equally relevant for absorption, too. For this reason, excitation polarization modulation depth M_E can be used as a measure of chain alignment: if $M_E = 1$, the chain is perfectly aligned, and if $M_E = 0$ — misaligned, with all the intermediate situations possible. The problem with this approach is that chains of very different conformations can have the same M_E , so, M_E is not informative for any *particular* single chain. However, histograms of occurrence of M_E values can be more useful, because for them this problem of conformation randomness is averaged out and diminished.

Also of interest is fluorescence polarization modulation depth M_F . If there is no energy transfer, M_F and M_E should be the same, but if energy transfer does occur, M_F can be different from M_E . In Article V we showed that from a scatter-plot of M_F against M_E for an ensemble of single chains one can make an estimate of the average number of emitters in a chain. However, if we only compare the modulation depths, the phase information is not be used. So, it can be even more

informative to use a method where all the possible steady-state polarization information is utilized. The method that we have found for that (Article VI) is based on measuring fluorescence intensity as a function of excitation and fluorescence polarization angles simultaneously. The result of such a measurement, being a function of two arguments, can be presented as a 2D plot. Examples of experimental polarization 2D plots are shown in Fig. 4.11.

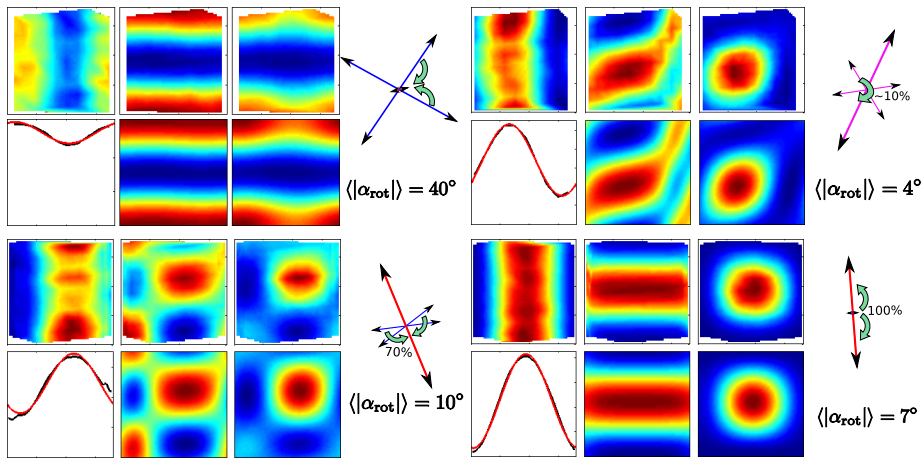


Figure 4.11: Examples of experimental 2D plots and their model fits.

These 2D plots contain all the steady state polarization information about a sample (can be a single molecule or any other photoluminescent object, not necessarily microscopic), and it is interesting to know how much precisely. That is, how many degrees of freedom do the polarization properties have? We have found a simplest model system of 3 symmetric dipole emitters with energy transfer (Article VI, Fig. 4) that could simulate the steady-state polarization properties of any experimental sample we have tested. It is a convenient way of formalizing the results of these measurements. Besides, it showed that the 2D polarization properties have precisely 8 degrees of freedom.

Another outcome of the technique is an ability to characterize energy transfer in a sample. More precisely, a “rotational component” of it, because only energy transfer resulting in a net rotation of exciton transition dipole orientations can be detected with a polarization-sensitive technique. We chose to characterize this rotation with an average rotation angle $\langle |\alpha_{\text{rot}}| \rangle$ and found that $\langle |\alpha_{\text{rot}}| \rangle$ is clearly dependent on sample structure (single chains vs. chain aggregates), solvent (toluene vs. chloroform) and temperature (Article VI).

Chapter 5

Modelling and simulations

This is a short “bonus” chapter about work in progress, intended to provide an information supplementary to Article VII where it is described in more detail.

5.1 Monte Carlo simulation of polymer chain conformations

The MEH-PPV polymer chains that we dealt with experimentally were rather long (~ 1000 monomer units) with molecular weight of ~ 200 kDa. These are very complicated systems, and modern sophisticated approaches of quantum chemistry and molecular dynamics are not computationally feasible for them yet. Therefore, one has to limit the realism of a description and simplify the polymer models as much as possible. One way to do that is to represent a chain as a sequence of beads with bonds between them and introduce interaction between the beads and bending potential for the bonds. To simplify the computational task even further, the bead coordinates can be restricted to a rectangular lattice. The conformation can then be simulated through a large series (2.5×10^7 in our case) of Monte Carlo steps. Using this approach, we were able to simulate a “synthesis” of 1000-monomer polymer chains in solution with a “production” rate of 1 chain per hour on a single Pentium IV processor (Article VII). By tuning the model parameters one could adjust solubility and stiffness of the chain and obtain different chain conformations. Two examples — a collapsed conformation due to bad solubility and an unfolded conformation with defects — are shown in Fig. 5.1. The scale is not the same on the figure, because the unfolded molecule image was rendered from a larger distance than that of the collapsed one, which is zoomed in to see the details better.

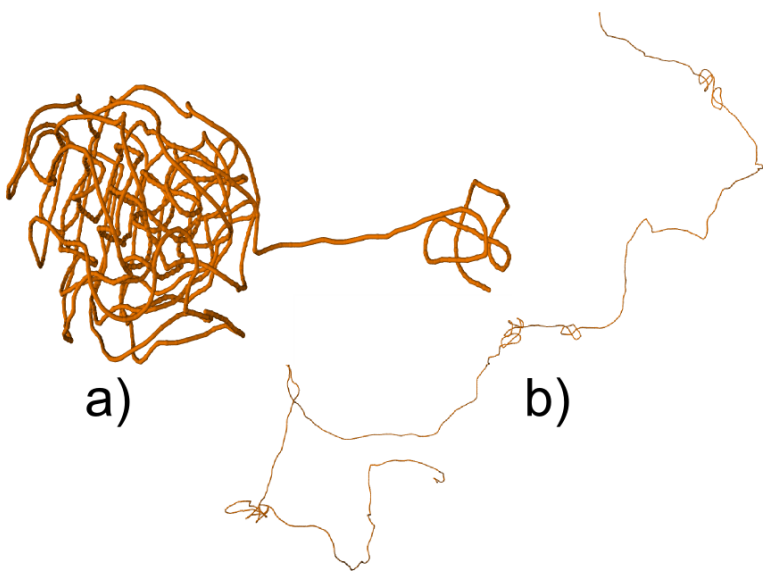


Figure 5.1: Examples of simulated polymer chain conformations. The image scale is different for the two examples.

5.2 Simulations of energy transfer in conjugated polymer chains

The spectral properties of a conjugated polymer chain are determined by the spectroscopic units that it contains. To mimic the spectroscopic units, the artificial chains were chopped into pieces by using a simple geometric criterion: as soon as a monomer along the chain deviated from the first monomer of a spectroscopic unit by an angle larger than some threshold value, it was declared to be the beginning of another spectroscopic unit.

The next task was to determine the spectroscopic properties of the chromophore as a function of its length. The details of how it was done are described in Section III of Article VII, and the resulting set of absorption spectra is presented in (Fig. 5.2). In a real chain chromophores do not have discrete lengths. Besides, inhomogeneous broadening is present and shifts the spectra of individual chromophores randomly. To account for that in a simple way, instead of broadening the spectra or randomly shifting them, the excitation was broadened. The center of the excitation spectrum was 19450 cm^{-1} , which corresponds to 514 nm (Ar^+ -laser line used in the experiments).

When the spectra of the chromophores are known, the excitation energy transfer rates between them can be calculated using the Förster's theory. When the rates are known, any other photophysical process

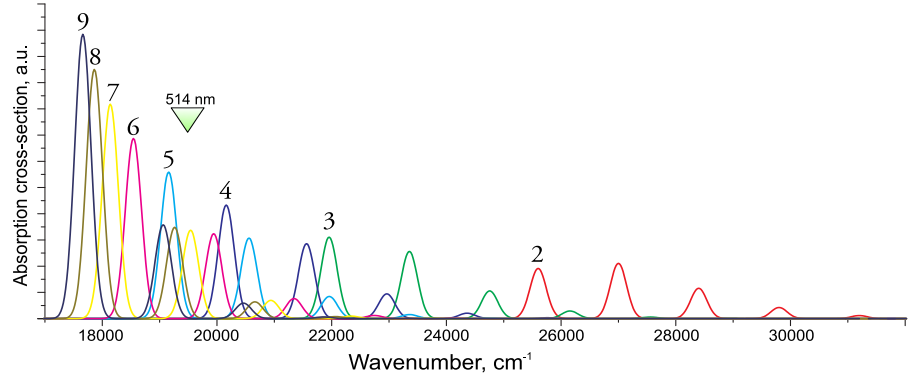


Figure 5.2: Model absorption spectra of MEH-PPV chromophores of different length in monomeric units (marked on the plots).

or property (within the scope of the model) can be simulated: fluorescence kinetics, time-resolved fluorescence spectrum, absorption spectrum, polarization properties, etc. We have used the model to simulate the results of the 2D polarization imaging technique (Section 4.5 and Article VI) of a series of the model polymer chain conformations. Two examples (simulated for the chains from Fig. 5.1) are shown in Fig. 5.3.

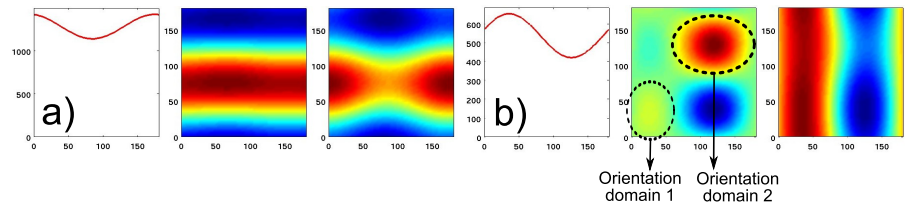


Figure 5.3: Simulated polarization 2D plots of the molecules from Fig. 5.1.

The left plot corresponds to the highly folded molecule, and it shows no dependence of fluorescence polarization on the excitation polarization angle (horizontal middle plot). This is in agreement with a natural assumption that in a collapsed molecule energy transfer is facilitated, and it results in efficient funneling (or redistribution) of excitations to the same set of chromophores, independently of the initial occupation probabilities. The right plot (Fig. 5.1b) corresponds to the unfolded chain with staircase-like shape and knot-like defects (Fig. 5.1b). One can see how the chain conformation shows up in this 2D plot by comparing it with the similar plot from the experiment (Fig. 4.11, bottom left example). Such structure of the middle (the intensity-normalized)

plot is inherent to molecules with two orthogonal orientation domains with zero or limited ET between them. In the case of this simulated chain the staircase-like structure serves as these two domains, and the knot-like defects — as separating chromophores with higher transition energy, which prevent ET across them from one straight segment to the next.

Bibliography

- [1] Moerner, W.; Kador, L. *Phys. Rev. Lett.* **1989**, 62(21), 2535–2538.
- [2] Orrit, M.; Bernard, J. *Phys. Rev. Lett.* **1990**, 65(21), 2716–2719.
- [3] Basche, T.; Kummer, S.; Brauchle, C. *Nature* **1995**, 373(6510), 132–134.
- [4] Ambrose, W.; Moerner, W. *Nature* **1991**, 349(6306), 225–227.
- [5] Lu, H.; Xie, X. *Nature* **1997**, 385(6612), 143–146.
- [6] Chiang, C.; Fincher, C.; Park, Y.; Heeger, A.; Shirakawa, H.; Louis, E.; Gau, S.; MacDiarmid, A. *Phys. Rev. Lett.* **1977**, 39(17), 1098–1101.
- [7] Shirakawa, H.; Louis, E.; MacDiarmid, A.; Chiang, C.; Heeger, A. *J. Chem. Soc. Chem. Comm.* **1977**, (16), 578–580.
- [8] Heeger, A. *Angew. Chem. Int. Edit.* **2001**, 40(14), 2591–2611.
- [9] Dimitrakopoulos, C. D.; Malenfant, P. R. L. *Adv. Mater.* **2002**, 14(2), 99.
- [10] Coakley, K. M.; McGehee, M. D. *Chem. Mater.* **2004**, 16, 4533–4542.
- [11] Shirota, Y. *J. Mater. Chem.* **2000**, 10(1), 1–25.
- [12] Pope, M.; Swenberg, C. *Electronic Processes in Organic Crystals and Polymers*, Vol. 2; Oxford University Press: New York, 1999.
- [13] Chang, R.; Hsu, J.; Fann, W.; Liang, K.; Chiang, C.; Hayashi, M.; Yu, J.; Lin, S.; Chang, E.; Chuang, K.; Chen, S. *Chem. Phys. Lett.* **2000**, 317(1-2), 142–152.
- [14] Graham, S.; Bradley, D.; Friend, R.; Spangler, C. *Synthetic Met.* **1991**, 41(3), 1277–1280.
- [15] Bredas, J.; Cornil, J.; Beljonne, D.; dos Santos, D.; Shuai, Z. *Accounts Chem. Res.* **1999**, 32(3), 267–276.

- [16] Van den Bout, D.; Yip, W.; Hu, D.; Fu, D.; Swager, T.; Barbara, P. *Science* **1997**, 277(5329), 1074–1077.
- [17] Yu, J.; Hu, D.; Barbara, P. *Science* **2000**, 289(5483), 1327–1330.
- [18] Huser, T.; Yan, M.; Rothberg, L. *Proc. Nat. Acad. Sci. USA* **2000**, 97(21), 11187–11191.
- [19] Rønne, C.; Trägårdh, J.; Hessman, D.; Sundström, V. *Chem. Phys. Lett.* **2004**, 388(1-3), 40–45.
- [20] Yu, Z.; Barbara, P. *J. Phys. Chem. B* **2004**, 108(31), 11321–11326.
- [21] Schindler, F.; Lupton, J.; Feldmann, J.; Scherf, U. *Proc. Nat. Acad. Sci. USA* **2004**, 101(41), 14695–14700.
- [22] Mirzov, O.; Pullerits, T.; Cichos, F.; von Borczyskowski, C.; Scheblykin, I. *Chem. Phys. Lett.* **2005**, 408(4-6), 317–321.
- [23] Moerner, W.; Fromm, D. *Rev. Sci. Instrum.* **2003**, 74(8), 3597–3619.
- [24] Press, W.; Teukolsky, S.; Vetterling, W.; Flannery, B. *Numerical Recipes in C - The Art of Scientific Computing*; Cambridge University Press, 1992.
- [25] Atkins, P.; Friedman, R. In *Molecular Quantum Mechanics*, Vol. 3; Oxford University Press: New York, 1997; pages 389–392.
- [26] Movaghfar, B.; Grunewald, M.; Ries, B.; Bässler, H.; Wurtz, D. *Phys. Rev. B* **1986**, 33(8), 5545–5554.
- [27] Schwartz, B. *Annu. Rev. Phys. Chem.* **2003**, 54, 141–172.

Acknowledgements

It has been four and a half years since I joined the Department of Chemical Physics, as an exchange student first and as a PhD student later. This is a noticeable part of life, and so has been, I believe, my development both as a scientist and as a person. But we people are social beings, and it never happens that we develop ourselves alone by ourselves. There always have to be other people that teach us and learn from us, help us and get help from us, share their and appreciate our thoughts and ideas, comfort us and get comforted, inspire us and get inspired. It is those people whose guidance, help, inspiration, friendship and love I would like to acknowledge here.

First of all, my closest collaborator and supervisor Dr. Ivan Scheblykin should be mentioned. Thank you, Vanja, for the great working conditions you've created in the SMS group, your numerous experimental innovations and developments and your stimulating scientific enterprise.

Equally important was the support and understanding of my main supervisor, Prof. Villy Sundström, who with his empathic approach to people is giving a healthy atmosphere and efficiency to the Department. Thank you for encouragement and help, Villy.

Big thanks go to Drs. Arkady Yartsev and Tõnu Pullerits — the other two pillars that the excellence of the optical part of the Department rests upon. Thank you for all your feedback and advice, for all the scientific and other discussions we had.

Also very important and enjoyable was collaboration with the other members of the SMS group: Cecilie, Ralph, Daniel, Hongzhen, Magdalena, Seyed, Robbert. Thank you, guys, it was great working with you!

Thanks to all of my office mates for great company: Kim, Gabor, Juan-Angel, Susanne, Alexandra, Benjamin, Erik, Jakob! I'm also grateful to Han-Kwang for his influence on me in the area of open-source software.

And of course, I'm very grateful to all the other members of the Department (too numerous to be listed), both former and present, for being nice people and good colleagues. Thank you for all the Fikas, lunches, Monday meetings, discussions, Spring and Autumn trips!

Work is not everything people do, and I'm happy to have also met many good friends outside the Department while working in Lund (in roughly chronological order): Yuri & Oksana, Anton, Yulia (a few of them ☺), Dima, Kostya, Vaida, Vanja & Irina, Taras & Marina, Ira, Sveta I., Sasha, Karen & Georgij, Sergey, Valeria, Marina K., Audrius & Natalia, Gvidas, Eligijus, Sveta L., Aliaksei, Andrei, Elvira, Terese, and my Natasha. Thank you for our skiing, hiking and road trips, picnics, visits to sauna, movie nights, birthday, house warming, PhD defence and all other sorts of parties, and for a lot of conversation about Life, the Universe and Everything ☺

Last but not least, I want to thank my parents for making me what I am and for their constant love and support. And thank you, Natasha, for being by my side.

Article I

O. Mirzov, I. G. Scheblykin

"Photoluminescence spectra of a conjugated polymer: from films and solutions to single molecules"

Reprinted with permission from *Phys.Chem.Chem.Phys.*, **2006**, 8, 5569
(cover article)

(Removed from this pdf to prevent publishing copyrighted materials online.)

Article II

T. Pullerits, O. Mirzov, and I. G. Scheblykin

“Conformational Fluctuations and Large Fluorescence Spectral Diffusion in Conjugated Polymer Single Chains at Low Temperatures”

Reprinted with permission from *J.Phys.Chem.B*, **2005**, *109*, 19099

(Removed from this pdf to prevent publishing copyrighted materials online.)

Article III

O. Mirzov, F. Cichos, C. von Borczyskowski, I. G. Scheblykin

"Direct exciton quenching in single molecules of MEH-PPV at 77 K"

Reprinted with permission from *Chem.Phys.Lett.*, **2004**, 386, 286

(Removed from this pdf to prevent publishing copyrighted materials online.)

Article IV

O. Mirzov, F. Cichos, C. von Borczyskowski, I. Scheblykin
"Fluorescence blinking in MEH-PPV single molecules at low temperature"

Reprinted with permission from *J.Lum.*, **2005**, *112*, 353
(Removed from this pdf to prevent publishing copyrighted materials online.)

Article V

H. Lin, S. R. Tabaei, D. Thomsson, O. Mirzov, P.-O. Larsson, I. G. Scheblykin

"Fluorescence Blinking, Exciton Dynamics and Energy Transfer Domains in Single Conjugated Polymer Chains"

accepted for publication in JACS

(Removed from this pdf to prevent publishing copyrighted materials online.)

Article VI

O. Mirzov, R. Bloem, P. R. Hania, D. Thomsson, H. Lin, and I. G. Scheblakin

“2D polarisation single molecule imaging of multichromophoric systems with energy transfer”

Manuscript

(Removed from this pdf to prevent publishing copyrighted materials online.)

Article VII

O. Mirzov and I. G. Scheblykin

"Single conjugated polymer chain conformation and excitation energy transfer simulations"

Manuscript

Single conjugated polymer chain conformation and excitation energy transfer simulations

O. Mirzov and I.G. Scheblykin*

Chemical Physics, Lund University, P.O.Box 124, 22100 Lund, Sweden

(Dated: April 16, 2008)

I. INTRODUCTION

Long π -conjugated polymer chains are complicated systems whose detailed quantum-chemical analysis is far beyond what is possible at the moment. So far, quantum chemical calculations have been successfully applied only to oligomers¹. Moreover, a very short polymer chain in a bad solvent presents a computationally expensive problem even for a molecular dynamics simulation². On the other hand, it is of great interest to find a way to simulate conjugated chain conformation as a function of sample preparation conditions (*e.g.* solvent) and calculate photophysical properties (*e.g.* absorption spectrum, polarization properties, fluorescence kinetics, time-resolved fluorescence spectrum, etc.) as a function of the conformation. This would give us an ability to establish a correlation or dependence between the photophysical properties and sample preparation conditions, and possibly allow us to infer something about a chain conformation from the experimental observations. The only feasible way to achieve this goal for a long (\sim 1000 monomer units) π -conjugated polymer chain is to simplify the models as much as possible.

One computationally cheap approach to simulate polymer chain conformations is the bond fluctuation method³. It has been followed by Hu et al.⁴ with some modifications that allowed the authors to simulate chain conformations (100 monomer units) for different values of chain stiffness and different solvents, and to derive histograms of polarization anisotropy in absorption for the different conformation sets. Excitation energy transfer and fluorescent properties were not dealt with.

The modern descriptions of intrachain excitation energy transfer and fluorescent properties of conjugated polymer chains are based on viewing the chain as a set of chromophores spanning its segments⁵. Therefore, the approach to simulating polymer chain photophysics can consist in evaluating spectral properties of the spectroscopic units, energy hopping rates between them and deriving the photophysical properties from the rates and the properties of the chromophores. This general approach was used in some previous work^{6–10}. However, in all this work the chain conformation was treated rather crudely — with static Monte Carlo growth and similar techniques.

With this contribution, we present a technique and a model suitable for simulating the photophysical properties of large (1000 monomer units) phenylenevinylene-based conjugated polymer chains. A further extension of the bond fluctuation method is used to generate the chain

conformations and study their dependence on a solvent, chain stiffness and the number of chemical defects. Thus generated polymer chains were segmented into spectroscopic units — separate chromophores whose spectral properties were derived from the exciton theory. Excitation energy transfer rates between them were calculated using the line-dipole enhancement¹¹ of the Förster theory.

The technique has been used to simulate a series of polymer chain conformations and to calculate for them the results of a new technique — 2D polarization single-molecule imaging¹². The results are discussed and compared with experiment. Besides, a simulation of fluorescence kinetics and its dependence on the presence of quenchers and their positions on the chain is demonstrated.

II. CHAIN CONFORMATION SIMULATIONS

A. Representation of a polymer chain

Since we are interested in simulating conformations of a polymer chain with the length of \sim 1000 monomers, we need to simplify the model of the polymer as much as possible to bring the computational cost down to a reasonable level. Fortunately, torsional degrees of freedom (*syn-* and *anti-* conformations, Fig. 1 a,b,c) do not have a profound effect on the conformation of a PPV-based polymer chain: such a defect changes the orientation of the chain but slightly, and it is restored back after another defect (Fig. 1b). This feature of PPV chain is not inherent to polythiophenes⁹. However, tetrahedral defects (Fig. 1d) do matter, and therefore we can follow the approach taken by Hu et al.⁴ and adopt the beads-on-a-chain model of a polymer, with equilibrium bond-to-bond angle equal to zero for normal monomers and $180^\circ - 109.5^\circ$ for the tetrahedral defect sites. In this simplified representation, every bead has only three degrees of freedom.

B. The bond fluctuation method

In this work we have used the bond fluctuation method³ modified with bending and stretching potentials and interactions between monomers (Subsection II C). The bond fluctuation method³ is a lattice Monte Carlo algorithm whose idea consists in allowing the distance between adjacent beads (*i.e.* the “bond length”) to vary

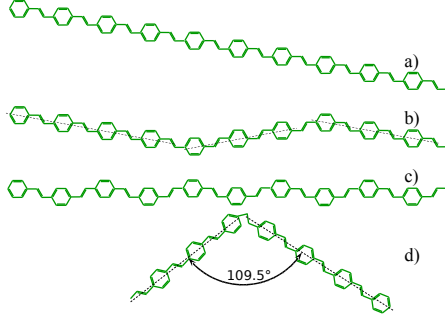


FIG. 1: *Syn-* and *anti-* configurations of PPV — all *anti* (a), random *syn* and *anti* mixture (b) and all *syn* (c) — don't have a strong effect on the chain conformation, in contrast to tetrahedral defects (d).

within some range and keeping the distance between any two beads above some limit. The range and the limit are chosen so as to avoid bond cuts and ensure self-avoiding walk at the same time. This approach makes the simulated chain more mobile in comparison with the older Monte Carlo algorithms^{13,14} where monomers were represented with strictly defined rather than variable-size elements.

The algorithm consists in applying a series of Monte Carlo steps to the chain of beads positioned at the discrete lattice points. During each step, one bead is randomly selected. After that one of the directions is chosen and checked whether it satisfies the imposed geometric constraints (Fig. 2). If the chosen direction is geometri-

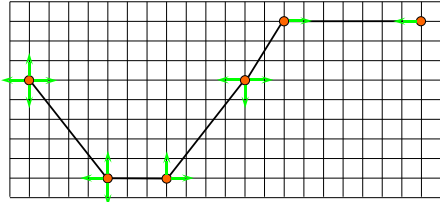


FIG. 2: The bond fluctuation method, illustrated for the 2D case for clarity. The geometrically plausible moves are shown for the case of $3 \leq l \leq 7$ constraint.

cally plausible, the monomer jumps the distance of one lattice unit into the chosen direction, otherwise nothing happens. After this the algorithm goes on to the next Monte Carlo step. We used the lattice unit length of 1.2 Å and the constraint on the monomer length l was $3 \leq l \leq 7$ (in lattice units), thus the average monomer length was 5 lattice units or 0.6 nm.

C. Interactions, bending and stretching

The bond fluctuation method (Subsection II B) was created for simulating Brownian motion dynamics of a polymer chain in a good solvent. The beads were assumed to represent Kuhn's segments rather than monomer units, so the stiffness of the chain was not taken into account. However, to get some insight into the properties of π -conjugated polymers, we are interested in modelling a polymer chain with a certain stiffness placed into a certain solvent, and we want to be able to adjust the stiffness and “goodness” of the solvent. To do that, we must introduce a bending potential and interactions between the monomers. For these two elements of the model, we took an approach close to the one by Hu et al.⁴, but in our case the beads correspond to single monomer units rather than Kuhn's segments.

To model the intermonomer interactions, we have used the Lennard-Jones potential

$$E_{LJ}(r) = 4E_0 \left[\left(\frac{r_0}{r} \right)^{12} - \left(\frac{r_0}{r} \right)^6 \right] \quad (1)$$

which equals zero at the distance r_0 and has the minimum $-E_0$ at the distance $r_0\sqrt[6]{2}$ (Fig. 3).

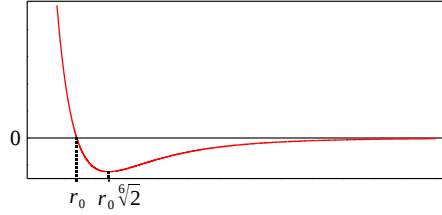


FIG. 3: The Lennard-Jones potential, reaching minimum at $r = r_0\sqrt[6]{2}$ and zero at $r = r_0$.

The bending potential intended to represent the stiffness of a chain has a simple form

$$E_{\text{bend}}(\alpha) = b\alpha^2, \quad (2)$$

where b is the bending constant and α is the deviation of the monomer-to-monomer angle from its equilibrium value.

To give the simulated chain a higher freedom (and consequently higher mobility) we have chosen to allow a very wide range for the monomer length l (from 3 to 7, see Subsection II B). However, so high range is very unphysical, so to correct that while retaining the conformational freedom we have also introduced a stretching potential:

$$E_{\text{str}}(\Delta l) = s(\Delta l)^2, \quad (3)$$

where Δl is the displacement of the monomer length l from the equilibrium value $l_{\text{equil}} = 5$ lattice units and s is the stretching constant.

D. “Synthesis” of a polymer chain

The introduction of bending, stretching and Lennard-Jones potentials (Subsection II C) into the bond fluctuation method (Subsection II B) leads us to modification of the way the monomer jumps are made. Now, instead of choosing the jump direction randomly, the choice is made based on the energy change ΔE that this jump would cause, so that the probability of every possible jump becomes

$$P_i = \frac{\exp(-\Delta E_i/k_B T)}{\sum_i \exp(-\Delta E_i/k_B T)}, \quad (4)$$

where T is the temperature, k_B is the Boltzmann constant and the index i enumerates all the geometrically plausible moves.

Now, one possible approach to simulating a chain conformation using the above model would be to generate a self-avoiding random walk conformation first, and then to “switch on” the potentials and apply a large number of Monte Carlo steps⁴. However, this approach has the serious drawback of starting from a certainly unphysical conformation with impossible bending angles. Therefore, we have decided to take another approach by “synthesizing” the chain during the simulation. We started with a single monomer and added other monomers one by one, “shaking” the chain after every addition with a fixed number of Monte Carlo steps per monomer. In this way, the physical time between the additions was kept constant, although the computational cost (and therefore time) of adding every new monomer grew proportionally with the chain length. When adding a new monomer, the place for the new node was selected among geometrically plausible ones with the probabilities given in Eq. 4. All the potentials were “switched on” during the whole simulation.

To summarize, the simulation algorithm can be roughly outlined as follows.

1. Start with one node at position $(0, 0, 0)$, potentials are on.
2. Randomly select a place for a new monomer, using the probabilities in Eq. 4.
3. Apply Monte Carlo steps, their number being the multiple of the current number of monomers and the number of steps per monomer which is fixed during the whole simulation.
4. Repeat the steps 2 and 3 until the desired number of monomers has been added.

E. Results

The method described above has been used to generate 90 polymer chains with different values of simulation parameters. The most crucial ones for conformation are the depth of the Lennard-Jones potential E_0 ,

the bending potential b and the percentage of tetrahedral defects in the chain. The bending potential was fixed at $b = 15 \text{ kT} \cdot \text{rad}^{-2}$, the defect percentage was either zero or 3% for different simulation batches, and E_0 was varied from 0 to $2kT$. The total number of Monte Carlo steps was 2.5×10^7 , which corresponded to 50 steps per monomer per every added monomer in the course of the “synthesis”. Thus, the first monomer was subjected to 50 000 steps during the simulation while the last — only to 50. The computational time for one chain was ~ 2500 seconds of single Pentium IV CPU time.

The most fundamental feature of polymer chain conformation is the ability of the chain to fold into collapsed structures and unfold into open, random-walk-like trajectories. The standard parameter used to characterize this aspect of conformation is the radius of gyration defined as

$$R_g^2 = \frac{1}{N} \sum_{i=1}^N (r_i - r_{\text{mean}})^2, \quad (5)$$

where r_i are the coordinates of the monomer units, N — their number, and r_{mean} is the mean monomer coordinate, which is naturally the chain’s center of mass. Fig. 4 presents the examples of extreme cases: very good and very bad solvent. The effect is clearly reflected in the values of R_g . It should be noted that the most compact conformation (such as Fig. 4c) corresponds to packing a 1000-monomer chain into a sphere with a diameter of ≈ 10 nm. It is easy to estimate¹⁵ that for the MEH-PPV polymer this corresponds to the density of a bulk material ($\sim 1 \text{ g/cm}^3$). This degree of packing was determined by the choice of the zero interaction distance of Lennard-Jones potential (Fig. 3) $r_0 = 2.1 \text{ nm}$.

The correlation between the interaction potential depth and the radius of gyration of the simulated chains is shown in Fig. 5 separately for the cases of chains with and without tetrahedral defects. The case of low E_0 corresponds to good solvents and the chains are mostly unfolded in this case, whereas at high E_0 the chains tend to collapse. The presence of defects clearly facilitates folding of a chain in most cases, which is reflected in the scatter-plot.

III. ENERGY TRANSFER SIMULATIONS

A. Spectroscopic units and their spectral properties

According to the currently accepted physical picture⁵, conjugated polymers can be viewed as consisting of multiple chromophores (also referred to as spectroscopic units) with a possibility of energy transfer between them. So, the first task in simulating the spectroscopic properties of the whole chain was to segment it into spectroscopic units and characterise them first. Since it is known^{5,16,17} that both conformational and chemical defects can disrupt the

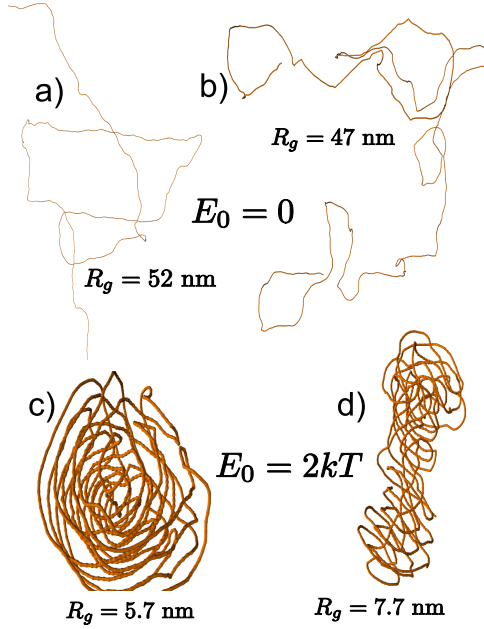


FIG. 4: Examples of simulated conformations for the case of zero (a,b) and high (c,d) intermonomer interaction potential depth. The image scale is different for these examples.

π -conjugation, and because chemical defects are reflected by the conformation in our chain model (Section II), we chose to use the following procedure for “chopping” the chain into individual chromophores. We started with the first monomer, then found the nearest along-the-chain neighbor that deviated higher than a certain angle from it, declared the latter to be the beginning of the next spectroscopic unit, and repeated the procedure. Formally, it can be expressed as

$$(\vec{\tau}_{i,n} \cdot \vec{\tau}_{f,n}) > c_{min} \geq (\vec{\tau}_{i,n} \cdot \vec{\tau}_{i,n+1}), \quad (6)$$

where $\vec{\tau}_{i,k}$ and $\vec{\tau}_{f,k}$ stand for the unit vectors along the initial and the final monomers of k th chromophore, respectively, and c_{min} is a model parameter. The result of this procedure is a segmentation of the chain into sequential spectroscopic units, each consisting of an integer number of monomers.

To assess the spectroscopic properties of thus identified chromophores, the results of the exciton theory were used¹⁸. First of all, the wavenumber of the vertical 0–0 vibronic transition as a function of the number of monomers N_{mon} within the chromophore was described

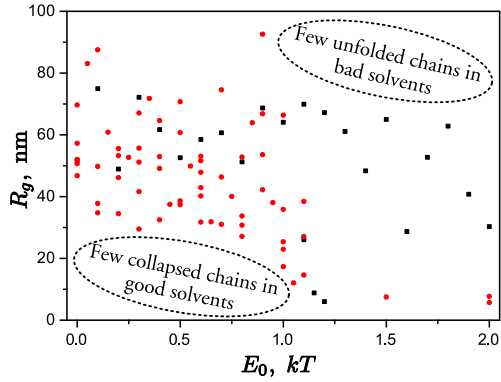


FIG. 5: Correlation between the interaction potential depth E_0 and radii of gyration R_g of the simulated polymer chains with (circles) and without (squares) tetrahedral defects.

as

$$\tilde{\nu}_{00}(N_{\text{mon}}) = \tilde{\nu}_{00}^{\text{mon}} + 2\beta \cos\left(\frac{\pi}{N_{\text{mon}} + 1}\right), \quad (7)$$

where for MEH-PPV¹⁸ $\tilde{\nu}_{00}^{\text{mon}} = 34400 \text{ cm}^{-1}$ and $\beta = -8800 \text{ cm}^{-1}$.

Several vibronic modes have been identified for the $\pi-\pi^*$ transition of MEH-PPV¹⁹. However, since the high-energy modes are close, it is sufficient for our purposes to describe the high-energy modes with a single mode and reflect the presence of the low-energy ones with a Stokes shift and a spectral broadening, assuming their energy $\lesssim kT$. In this way, we describe the absorption and fluorescence spectra of our chromophores as a simple single-mode progression

$$I_{0 \rightarrow n} = \frac{H^n \exp(-H)}{n!}, \quad (8)$$

where H is the Huang-Rhys factor of the mode that depends on N_{mon} as¹⁸

$$H(N_{\text{mon}}) = \frac{3H_{\text{mon}}}{2(N_{\text{mon}} + 1)}, \quad N_{\text{mon}} > 1, \quad (9)$$

where H_{mon} is a model parameter — the Huang-Rhys factor of a chromophore containing only one monomer unit. The components of the vibronic progression are separated by the vibrational energy of the main mode E_{vibr} which is another model parameter that needs to be fixed.

The low-energy modes appear in the model only via a broadening of the high-energy mode vibronic transitions and via the symmetric Stokes shift of the low-energy mode vertical transitions in absorption and emission with respect to the 0–0 transition (Fig. 6). All the low-energy

- ⁷ S. Westenhoff, C. Daniel, R. Friend, C. Silva, V. Sundstrom, and A. Yartsev, *J. Chem. Phys.* **122**, 094903 (2005).
- ⁸ S. Westenhoff, W. Beenken, A. Yartsev, and N. Greenham, *J. Chem. Phys.* **125**, 154903 (2006).
- ⁹ S. Westenhoff, W. Beenken, R. Friend, N. Greenham, A. Yartsev, and V. Sundstrom, *Phys. Rev. Lett.* **97**, 166804 (2006).
- ¹⁰ E. Hennebicq, G. Pourtois, G. Scholes, L. Herz, D. Russell, C. Silva, S. Setayesh, A. Grimsdale, K. Mullen, J. Bredas, et al., *J. Am. Chem. Soc.* **127**, 4744 (2005).
- ¹¹ W. Beenken and T. Pullerits, *J. Chem. Phys.* **120**, 2490 (2004).
- ¹² See Article VI.
- ¹³ P. H. Verdier and W. H. Stockmayer, *Journal Of Chemical Physics* **36**, 227 (1962).
- ¹⁴ K. Kremer and K. Binder, *Computer Physics Reports* **7**, 259 (1988).
- ¹⁵ O. Mirzov, F. Cichos, C. von Borczyskowski, and I. Scheblykin, *Chem. Phys. Lett.* **386**, 286 (2004).
- ¹⁶ W. Beenken and T. Pullerits, *J. Phys. Chem. B* **108**, 6164 (2004).
- ¹⁷ S. Grimm, A. Tabatabai, A. Scherer, J. Michaelis, and I. Frank, *Journal Of Physical Chemistry B* **111**, 12053 (2007).
- ¹⁸ R. Chang, J. Hsu, W. Fann, K. Liang, C. Chiang, M. Hayashi, J. Yu, S. Lin, E. Chang, K. Chuang, et al., *Chem. Phys. Lett.* **317**, 142 (2000).
- ¹⁹ F. Schindler and J. Lupton, *Chemphyschem* **6**, 926 (2005).
- ²⁰ V. May and O. Kühn, *Charge and Energy Transfer Dynamics in Molecular Systems* (Wiley-VCH, 2004), chap. 5.2.4 Absorption Coefficient for Harmonic Potential Energy Surfaces.
- ²¹ P. Atkins and R. Friedman, *Molecular Quantum Mechanics* (Oxford University Press, 2003), chap. Further information 17. Oscillator strength, p. 510.
- ²² P. Atkins and R. Friedman, *Molecular Quantum Mechanics* (Oxford University Press, 2003), chap. Chapter 6. Techniques of approximation, p. 196.
- ²³ V. Agranovich and M. Galanin, *Electronic Excitation Energy Transfer in Condensed Matter*, 3 (North Holland Pub. Co., 1982).
- ²⁴ T. Pullerits, S. Hess, J. L. Herek, and V. Sundstrom, *Journal Of Physical Chemistry B* **101**, 10560 (1997).
- ²⁵ T. Pullerits, K. J. Visscher, S. Hess, V. Sundström, A. Freiberg, K. Timpmann, and R. Vangronnelle, *Biophysical Journal* **66**, 236 (1994).
- ²⁶ I. Osad'ko, *Sov. Phys. Usp.* **22**, 311 (1979).
- ²⁷ See Article V.